Am J Cancer Res 2021;11(4):1600-1615
www.ajcr.us /ISSN:2156-6976/ajcr0124750

Original Article

New insight into the role of ANXA1 in melanoma progression: involvement of stromal expression in dissemination

Solène Delorme[1], Maud Privat[1,2], Nicolas Sonnier[1,2], Jacques Rouanet[1], Tiffany Witkowski[1], Myriam Kossai[1,3], Florence Mishellany[1,3], Nina Radosevic-Robin[1,3], Gaëtan Juban[4], Ioana Molnar[1,5], Mercedes Quintana[1], Françoise Degoul[1]

[1]Université Clermont Auvergne, INSERM, Imagerie Moléculaire et Stratégies Théranostiques, UMR1240, 58 Rue Montalembert, Clermont-Ferrand Cedex 63005, France; [2]Département d'Oncogénétique, Centre Jean Perrin, Clermont-Ferrand 63000, France; [3]Département de Pathologie, Centre Jean Perrin, Clermont-Ferrand 63000, France; [4]Institut NeuroMyoGène, Université Claude Bernard Lyon 1, CNRS UMR 5310, INSERM U1217, Université Lyon, Lyon 69008, France; [5]Département de Recherche Clinique et Innovation, Centre Jean Perrin, Clermont-Ferrand 63000, France

Received October 22, 2020; Accepted December 28, 2020; Epub April 15, 2021; Published April 30, 2021

Abstract: ANXA1, first described in the context of inflammation, appears to be deregulated in many cancers and increased in melanomas compared with melanocytes. To date, few studies have investigated the role of ANXA1 in melanoma progression. Furthermore, this protein is expressed by various cell types, including immune and endothelial cells. We therefore analyzed the specific roles of ANXA1 using melanoma and stromal cells in two human cell lines (A375-MA2 and SK-MEL-28) *in vitro* and in *Anxa1* null C57Bl6/J mice bearing B16Bl6 tumors. We report decreased proliferation in both ANXA1 siRNA A375-MA2 and SK-MEL-28, but cell-dependent effects of ANXA1 in migration *in vitro*. However, we also observed a significant decrease of B16Bl6 tumor growth associated with a reduction of Ki-67 positive cells in *Anxa1* null mice compared with wild-type mice. Interestingly, we also found a significant reduction of spontaneous metastases, which can be attributed to decreased angiogenesis concomitantly with greater immune cell presence in the *Anxa1* null stromal context. This study highlights the pejorative role of ANXA1 in both tumor and stromal cells in melanoma, due to its involvement in proliferation and angiogenesis.

Keywords: ANXA1, melanoma, migration, proliferation, metastases, angiogenesis, immune infiltrate

Introduction

Annexin A1 (ANXA1) is known as a protein involved in inflammation, decreasing neutrophil diapedesis to inflamed sites and inducing their apoptosis there [1]. This is mediated by extracellular forms of ANXA1, whose expression can be modified by glucocorticoids (GC). Macrophages can also produce ANXA1 in response to stimulation by GC, secreting ANXA1 in a paracrine or autocrine fashion and facilitating the engulfment of apoptotic cells [1]. The ANXA1 receptor currently described is formyl peptide receptor 2: FPR2 (also known as ALXR); it belongs to the FPR family whose canonic ligands are bacterial formylated peptides. ANXA1 has recently been shown to trigger a reparative macrophage function via FPR2, activating the AMPK pathway in a muscle injury model [2]. Besides its role in innate immunity, ANXA1 can boost adaptive immunity, as demonstrated by Dr. F. D'Acquisto [3]. Interestingly, in knockout (KO) mice infected with mycobacterium tuberculosis, a lack of ANXA1 decreased $CD8^+$ activation by DC [4]. Similarly, ANXA1 contributes to immunogenic cell death following certain cancer chemotherapies or radiotherapies [5-8].

During the last twenty years, ANXA1 has been highlighted as a biomarker for different cancers (see [9] for a review). As a potential consequence of its immunomodulatory and additional roles, ANXA1 expression is either reduced or increased in tumors depending on the type of

cancer. For some locations, such as breast cancers, conflicting results have been reported [10]. Our team observed increased expression of ANXA1 in invasive melanomas in preclinical models, which was confirmed on a patient cohort [11, 12]. Our hypothesis is that external ANXA1, either linked to the plasma membrane or secreted, can activate invasive pathways in melanoma cells via FPR. This has also been proposed for other malignancies, such as breast, gastric or prostate cancers, and gliomas (see [13] for a review). Our team and others have shown that manipulation of the level of ANXA1 in tumors can affect their metastatic behavior. More specifically, decreasing tumor ANXA1 induces a lower rate of metastases in 4T1 murine breast cells implanted in NOD2SCID mice [14], in syngeneic murine melanoma B16Bl6 [12] and in MiaPaca2 pancreatic tumors in SCID mice [15]. Interestingly, decreasing stromal ANXA1 is associated with slower tumor growth in B16, and reduced metastases in LLC and 4T1 tumors in syngeneic models [16, 17]. These later observations have been linked to decreased angiogenesis, considering the presence of ANXA1 as a pivotal clue for vasculature walls in tumors [18], and to its immunomodulatory role, leading to a M1 phenotype for tumor-associated macrophages (TAMs) [16].

Altogether, these data encouraged us to investigate the involvement of tumoral and stromal ANXA1 in melanoma progression in more detail. To improve our knowledge on ANXA1 in human melanomas, we selected two aggressive cell lines, A372-MA2 and SK-MEL-28, to assess the role of ANXA1 on their migrating properties using exogenous Ac2-26 peptide mimicking the ANXA1 amino-terminus (Nter) domain or siRNA-specific ANXA1 knockdown. Furthermore, considering melanoma, the role of stromal ANXA1 merits further attention as the reported results were obtained on a B16 cell line without ANXA1 expression and unable to metastasize [17]. We therefore investigated the effect of stromal ANXA1 on tumor growth and on the occurrence of metastases in a B16Bl6-/C57Bl6/J model using *Anxa1* KO mice. Our results suggest that tumoral ANXA1 is involved in the proliferation of human melanomas and, depending on the cell line, in *in vitro* migration. They also support the notion that stromal ANXA1 plays an important role in melanoma development and dissemination *in vivo*, probably through its involvement in tumor proliferation and angiogenesis.

Materials and methods

Cell cultures and reagent

Human melanomas SK-MEL-3 (derived from lymph node metastasis of a female patient), SK-MEL-28 (derived from lymph node metastasis of a male patient) and A375-MA2 (derived from a non-metastatic cutaneous melanoma, further selected to become metastatic), were obtained from the American Type Culture Collection (ATCC). The murine B16Bl6 cell line came from Professor Fidler's lab (Texas University, Houston, USA). B16Bl6-luc cells expressing the luciferase gene were engineered in our laboratory by Dr. Claire Viallard. A375-MA2 and B16Bl6 were cultured in DMEM-Glutamax (31966-021, Invitrogen) with 10% fetal calf serum (FCS, CVFSVF00-01, Eurobio), SK-MEL-3 in McCOY'S 5A (26600-023, Invitrogen) with 15% FCS and SK-MEL-28 in MEM-Glutamax (41090028, Invitrogen) with 10% FCS. All the media were supplemented with 4 µg/mL gentamycin (15750-037, Invitrogen). The cells were grown at 37°C in a humid atmosphere containing 5% CO_2. The cells were treated with the peptide Ac2-26, which mimics the Nter domain of ANXA1 at 10 µM (1845, Tocris).

ANXA1 expression analysis by RT-qPCR using the TaqMan method

Total RNA was extracted from the cultured cells (SK-MEL-3, SK-MEL-28, A375-MA2) according to the manufacturer's instructions using an RNeasy mini kit (Qiagen). Samples were then quantified and RNA integrity was checked with the Agilent 2100 bioanalyzer using Agilent RNA 6000 nano kits (Agilent Technologies). RNA was reverse-transcribed from 1 µg RNA with a high-capacity cDNA reverse transcription kit (Applied Biosystems), according to the protocol supplied by the manufacturer. Reverse transcription was performed as follows: 10 min at 25°C, 120 min at 37°C and 5 min at 85°C. Real-time PCR using the TaqMan method was performed on 25 ng cDNA. The *UBC* gene was used as an endogenous control. The following primers and TaqMan probes, dye-labeled with FAM-MGB (VIC-MGB for

UBC), were used in the reaction: Hs001675-49_m1 for *ANXA1* and Hs01871556_s1 for *UBC*. The cycling parameters consisted of a first step at 50°C for 2 min and at 95°C for 10 min, followed by 40 cycles at 95°C for 15 sec and 60°C for 1 min. Three experimental replicates were performed. Cycle thresholds were analyzed with SDS2.4 and RQ Manager 1.2 software. Relative quantification was carried out using the $2^{-\Delta\Delta Ct}$ method.

Cell lysate and supernatant analysis of ANXA1 level by western blotting

The cells were seeded at 2×10^5 cells per well in six well plates for 24 hours. After three washes with DPBS (Dulbecco's phosphate-buffered saline), the supernatants were removed and replaced with 1 mL OptiMEM (31985-047, Invitrogen) containing 0.9 mM $CaCl_2$ (C4901, Sigma-Aldrich) and supplemented or not with a calcium chelator EGTA (E-4378, Sigma-Aldrich). The supernatant was collected and centrifuged at 460× g for 8 min at room temperature. The final supernatants were concentrated at 4°C using 10 kDa cut-off concentrators (Vivaspin 500, *VS0102,* Sartorius Stedim) to obtain a volume of less than 30 µL. Each supernatant sample was used in its entirety for the western blot analyses. The cells were lysed using an RIPA buffer containing 50 mM Trizma Base (T1503, Sigma-Aldrich) pH 7.5, 150 mM NaCl (7647-14-5, Merk), 1% NP40 (74385, Fluka), 0.5% sodium deoxycholate (D6750, Sigma-Aldrich), 0.1% SDS (19812323, Biosolve) and supplemented with 1× phosphatase and protease inhibitors (78443, ThermoFisher Scientific). After one centrifugation operation at 10000× g for 10 min at 4°C, protein concentration was estimated according to the Bradford protein assay (23200, Invitrogen). Equal amounts of protein from each sample (40 µg) were used for western blotting.

The proteins were separated through 4-15% SDS-PAGE (456-8084, Bio-Rad) and transferred onto nitrocellulose membranes (1620115, Bio-Rad). The membranes were blocked in TBS (pH 7.6, 200 mM Trizma Base and 1.5 M NaCl) containing Tween 20 (0.1%) (9005-64-5, FisherScientific) and 5% milk for 1 hour and incubated overnight at 4°C with anti-ANXA1 (rabbit polyclonal, 1:10000, 71-3400, Invitrogen). After three washes in TBS-Tween 20, the membranes were incubated 1.5 hours with horseradish peroxidase (HRP)-conjugated anti-rabbit IgG (1:5000, 4050-05, SouthernBiotech). After three washes, HRP activity was detected with Clarity™ Western ECL Substrate (170-5061, Bio-Rad) and a ChemiDoc™ MP Imaging System (Bio-Rad). Total protein normalization was applied using stain-free technology. A semi-quantitative measurement of protein level was obtained using Image Lab software (Bio-Rad).

ANXA1 level analysis by flow cytometry

SK-MEL-3, SK-MEL-28 and A375-MA2 cells were harvested at a number of 1×10^6 and stained with anti-ANXA1 (rabbit polyclonal, 1:500 for permeabilized and 1:100 for non-permeabilized cells, 71-3400, Invitrogen) to evaluate total and membrane expression. Isotype rabbit (EB-003-0110, Diagenode) antibody was used as a control. The cells were centrifuged briefly at 400× g for 5 min. To assess total expression, the cells were permeabilized with BD FACS™ permeabilizing solution 10X (347692, BD-Bioscience) for 10 min at room temperature and then centrifuged at 800× g for 5 min. For membrane ANXA1, the cells were not permeabilized. The pellets were incubated at 4°C for 30 min in a medium containing 1% BSA, 5 mM $CaCl_2$ (dilution buffer) and a primary antibody against ANXA1. The cells were then washed in a medium containing 1% FCS, 5 mM $CaCl_2$ (wash buffer) and incubated at 4°C for 30 min in a dilution buffer containing AlexaFluor™ 488 anti-rabbit (1/2000, A11008, Invitrogen). After one wash, the cells were stained with 4 µg/mL propidium iodide (PI) and analyzed on a BD LSRII flow cytometer (BD Biosciences, CICS_UCA PARTNER). FACSDiva data manager v8 software was used to determine the percentage of labelled cells and the mean fluorescence intensity (MFI).

Cell transfection with siRNA directed against ANXA1

The A375-MA2 and SK-MEL-28 cells were seeded at 2×10^5 and 1.5×10^5 cells per well, respectively, in six well plates for 24 hours. The cells were transfected with 25 pmol siRNA using the Lipofectamine® RNAiMAX reagent (13778-030, Invitrogen), according to the man-

ufacturer's instructions. The siRNA oligonucleotides for *ANXA1* (ON-TARGETplus Human ANXA1, L-011161-00-0005) and the control (ON-TARGETplus Non-targeting siRNAs, D-001810-0X) were purchased from Horizon™. The cells were harvested 48 hours post-transfection to verify ANXA1 depletion by western blotting.

Migration assay

Culture insert chamber migration assays were performed in a µDish 35 mm (81176, Ibidi®). The A375-MA2 and SK-MEL-28 cells were seeded at a density of 50,000 or 30,000 cells/70 µL, respectively, to each chamber of the culture insert. The transfected cells were seeded 24 hours after transfection. The cells were incubated for 24 hours to form confluent monolayers before removing the insert, leaving a cell-free gap of 500 µm without scratching the cell monolayer (48 hours post-transfection). The cells were rinsed three times with DPBS and fresh medium, with or without treatment, was added to the dish. For the siRNA experiments, 1% FCS medium was used to prevent cell proliferation. Images were taken at different times using an inverted microscope at 5× magnification (T0h corresponds to the time of insert removal and treatments). The experiments were run at least in triplicate for each condition. The gap area was estimated using Fiji software at different times and the percentage of wound closure was calculated with the following formula: [(T0h-Txh)/T0h] ×100.

Cell viability assay

To assess the cytotoxicity of the peptide Ac2-26 and the siANXA1 transfection, the resazurin reduction assay was used as an indicator of cell viability. Cytotoxicity was investigated 24 hours and 48 hours after treatment for the peptide and 48 hours and 72 hours post-transfection for the siANXA1. The control or transfected A375-MA2 (6×10^3 cells/well) and SK-MEL-28 (4×10^3 cells/well) cells were seeded in a 96-well plate in a culture medium. The cells were allowed to adhere for about 24 hours, then the non-transfected cells were treated with 10 µM Ac2-26. The cells were washed twice with DPBS and 25 µg/mL resazurin was added to each well. After 1-2 hours' incubation, fluorescence was measured with a microplate reader (Fluoroskan Ascent, Labsystems) using excitation and emission wavelengths of 530 nm and 590 nm, respectively. The percentage of living cells was determined relative to control conditions.

In vivo experimental models

All our experiments were conducted in compliance with the relevant guidelines and regulations and approved by both the local ethics committee of Clermont-Ferrand (C2E2A) and the French Ministry of Education and Research (approval n°17844). The C57BL6/J wild type (WT) mice were purchased from Charles River and the C57BL6/J *Anxa1* KO mice were supplied by Dr. Juban, Claude Bernard University, Lyon (CNRS UMR 5310, INSERM U1217) and correspond to the ANXA1-/- mice developed by Peretti's group [19]. Groups of mixed-sex animals were used, and animals of similar age and weight were selected.

Subcutaneous model: B16Bl6 murine melanoma cells suspended in DPBS were injected subcutaneously into the right flanks of the mice at the number of 2×10^5. Intratumoral injections of 20 µL NaCl were made at days 9 and 12 after cell implantation to promote the formation of metastases. The body weight of the mice and the tumor sizes were measured three times per week. The tumors were measured using a caliper and volume was calculated with the formula $(L\times S^2)/2$, where L and S are the largest and the smallest diameters in mm, respectively. Tumor growth was reported as the ratio (Vt-Vi)/Vi, where Vt is measured tumor volume on a given day and Vi initial volume (first day of measurement). The mice were sacrificed 19 days after cell inoculation. The tumors were removed, frozen in liquid nitrogen and stored at -80°C for protein and RNA extraction or fixed in formalin (HT501128, Sigma-Aldrich) for 24 hours and stored in 70% ethanol for the immunostaining analyses. The lung surface metastases visible under a binocular magnifier were counted.

Intravenous model: B16Bl6-luc cells suspended in DPBS were injected intravenously into the caudal veins of the mice at the number of 1.5×10^5. The body weight of the mice was measured three times per week. Lung tumor invasion was monitored using *in vivo* bioluminescence imaging on the day of cell injection (day 0) and at days 7, 14 and 18. The mice

Table 1. List of primers used in RT-qPCR studies

Genes	Forward primers 5' to 3'	Reverse primers 5' to 3'	Amplicon size (bp)	Annealing temperature (°C)
Cd45	ATGGTCCTCTGAATAAAGCCCA	TCAGCACTATTGGTAGGCTCC	70	60
Cd3	ATATCTCATTGCGGGACAGG	TCTGGGTGCTGGATAGAAGG	196	57
Cd8a	CTTGTGCCTCAAACTGCAAG	CCGCTAAAGGCAGTTCTCC	100	58
Grzb	GCTGCTCACTGTGAAGGAAGT	TGGGGAATGCATTTTACCAT	107	58
Ifnγ	AAAGAGATAATCTGGCTCTGC	GCTCTGAGACAATGAACGCT	229	57
Cd4	GCGAGAGTTCCCAGAAGAAG	AAACGATCAAACTGCGAAGG	126	58
Foxp3	CACCTGGAAGAATGCCATC	AGGGATTGGAGCACTTGTTG	146	57
Tbp	CCTTGTACCCTTCACCAATGAC	ACAGCCAAGATTCACGGTAGA	59	59

were injected intraperitoneally with 15 mg/mL luciferin (122799, PerkinElmer) and imaged 5 min thereafter. Average radiance of the lungs (p/s/cm^2/sr) was computed using Living Image software and radiance relative to day 0 was reported as the ratio (Rt-Ri)/Ri, where Rt is radiance on a given day and Ri initial radiance (day 0). The mice were sacrificed on day 18 after cell injection.

Tumor immune infiltrate analysis by RT-qPCR using the SYBR green method

The tumors were dissociated for RNA extraction with a GentleMacs using the RNA_02 program recommended for frozen tissues (130-093-235, Miltenyi Biotec). Total RNA was extracted according to the manufacturer's instructions, using NucleoSpin® RNA (740955.250, Macherey-Nagel™). Total RNA was quantified at 260 nm using a μDrop™ Plate (N12391, ThermoScientific) and RNA purity was measured using the absorbance ratio at 260 and 280 nm. RNA (1.5 μg) was reverse-transcribed with SuperScript™ IV VILO™ Master Mix with the ezDNase™ enzyme (ThermoFisher, Courtabœuf, France). Reverse transcription was performed as follows: 10 min at 25°C, 10 min at 50°C and 5 min at 85°C. qPCR-reactions were performed in triplicate with SYBR® Mix (KAPABIOSYSTEMS, Boston, USA) on a StepOnePlus device (Applied BioSystems, Foster City, USA) (**Table 1**). The cycling parameters consisted of a first step at 95°C for 3 min followed by 40 cycles at 95°C for 3 sec and at annealing temperature for 30 sec. PCR product specificity was checked according to the melting curve. The PCR cycles consisted of a step at 95°C for 15 sec followed by the dedicated annealing temperature for 1 min and a final step at 95°C for 15 sec. The cycle thresholds were analyzed using StepOne software. Relative quantification was determined according to the $2^{-\Delta\Delta Ct}$ method after normalizing the expression to that of *Tbp*.

VEGF dosage by enzyme-linked immunosorbent assay (ELISA)

Tumor protein extraction was performed with the TissueLyser system (Qiagen®) in a urea buffer containing 6 M urea (211823, Biosolve), 2.5 mM sodium pyruvate (11360-039, Invitrogen), 1 mM EDTA (15575-038, Invitrogen), 0.5% Triton X100 (T8787, Sigma) and 1× phosphatase and protease inhibitors (78443, ThermoFisher Scientific). The tumors were mechanically disrupted for 5 min at 30 Hz in 300 μL urea buffer using 5 mm beads. The extracts were separated by centrifugation (10 min, 14000× g, 4°C) and the supernatants run through a Bradford assay for protein quantification. ELISA analyses were run on around 20-30 μg of each extract using the Quantikine® ELISA kit (MMV00, R&DSYSTEMS®), according to the manufacturer's instructions.

Histological analysis

The tumors were embedded in paraffin and cut into 4 μm serial sections. They were immunostained using specific antibodies including anti-CD31 (ab28364, Abcam) and anti-Ki-67 (ab15580, Abcam) as follows. The sections were deparaffinized and rehydrated before being subjected to antigen retrieval using 10 mM Tris, 1 mM EDTA buffer pH 9 for CD31 or 10 mM citrate pH 6 for Ki-67. After two washes with water and one wash with PBS, endogenous peroxidases were inhibited using 0.3% hydrogen peroxide for 30 min (for Ki-67 staining only). After another PBS wash step, the

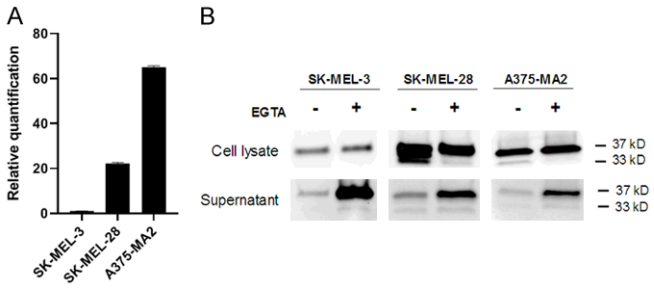

C

	ANXA1	
Cell lines	Total	Membrane
SK-MEL-3	99.7% (*933*)	13.5% (*140*)
SK-MEL-28	98.4% (*967*)	5.4% (*166*)
A375-MA2	99.7% (*2084*)	23.4% (*152*)

Figure 1. Comparison of total and secreted level of ANXA1 in different human cell lines. A. RT-qPCR analysis of ANXA1 in human melanoma cell lines. UBC was used as housekeeping gene and SK-MEL-3 as reference. B. Western blot analysis of ANXA1 in cell lysates and supernatants of human cells treated or not with the calcium chelator EGTA (2 mM). Total proteins were used as a loading control. Full lenght ANXA1 (37 kDa) and cleaved form (33 kDa) were detected. C. Flow cytometry analysis of total and membrane ANXA1. Results represent percentage of labelled cells (*MFI*).

sections were blocked 1 hour with 1% bovine serum albumin, before overnight incubation with anti-CD31 (1:100) or anti-Ki-67 (1:2000) at 4°C. The sections were then washed with PBS, followed by incubation for 1 hour with a secondary anti-rabbit antibody directly coupled with AlexaFluor 555 (1:1000, A21430, Invitrogen) or with a biotinylated antibody (1:500, 111-065-003, Jackson Immunoresearch). Two PBS washes were implemented before incubation with peroxidase-conjugated streptavidin (1:500, 016-030-084, Jackson Immunoresearch) for 30 min. After washing in PBS, the sections were incubated with Alexa Fluor™ 488 tyramide reagent (1:200, B40953, ThermoFisher Scientific) for 10 min, then washed twice in PBS. The nuclei were stained for 5 min in Hoechst 33342 solution (1:10000, H3570, Invitrogen) and coverslips were mounted in glycerol (50% v/v PBS). A Zeiss Axio Imager M2 was used to create a 4×4 mosaic image (16 tiles) with a ×20 objective to enable analysis of a wide field of each section. Fiji software was used to assess the number of vessels per tumor slide using quantitative analysis of CD31 on the mosaic images. The quantification of Ki-67 labelled cells required pathology expertise.

Statistical analyses

Statistical analyses were carried out on data from at least three independent experiments using GraphPad Prism v8.0 software. Data are presented as mean values ± standard deviation. Differences with a p value <0.05 were considered to be statistically significant.

To compare two different conditions (Ctrl vs peptide; siCTRL vs siANXA1; WT mice vs KO mice), a Student's t-test (with Welch's correction) was performed. When normality was not assumed, the nonparametric Mann-Whitney test was used. Significance was expressed relative to the corresponding control condition.

To evaluate the relationship between the absence of stromal ANXA1 and the number of measurable tumors or mice with lung metastases, a contingency table was created and a Chi-Square test carried out to determine statistical significance.

The effect of cell siANXA1 transfection on PCNA protein level was assessed by the protein level ratio of the siANXA1/siCTRL cells. One sample Student's t-test was performed with 1 (siCTRL/siCTRL) as the hypothetical value to assess ratio significance.

Results

Characterization of ANXA1 expression and localization in melanoma cell lines

Two as yet unexplored invasive human cell lines, A375-MA2 and SK-MEL-28 cells, present higher ANXA1 mRNA than the previously studied SK-MEL-3 [12] (**Figure 1A**). Cellular and membrane/secreted ANXA1 levels were assessed by western blotting and the use of EGTA enabled harvesting of the calcium-dependent, membrane-bound fraction. Similarly, cellular ANXA1 was higher in SK-MEL-28 and A375-MA2 than in SK-MEL-3 (**Figure 1B**). However, flow cytometry analyses (**Figure 1C**) showed

similar levels of total ANXA1, determined by mean fluorescence intensity (MFI), for SK-MEL-3 and SK-MEL-28. Interestingly, the ANXA1 level was twice as high in A375-MA2 compared with the other cell lines. Native (37 kDa) and cleaved (33 kDa) forms of ANXA1 were detected in the SK-MEL-28 and A375-MA2 cell lysates and supernatants (**Figure 1B**). To confirm the presence of membrane ANXA1, we used flow cytometry analysis with non-permeabilized cells (**Figure 1C**). A375-MA2 and SK-MEL-3 had the highest percentage of cells presenting membrane ANXA1. A375-MA2 and SK-MEL-28 expressed ANXA1 and presented extracellular forms of the protein: both membrane-bound and secreted. Taken together, these data confirm that these cell lines are relevant for investigation of the involvement of tumor ANXA1 in cell aggressiveness.

ANXA1 modulates melanoma proliferation and, in a cell line-dependent manner, migration in vitro

We determined the effect of endogenous ANXA1 in the proliferation and migration of SK-MEL-28 and A375-MA2 cells with specific siRNAs. After 48 hours of transfection, siRNA directed against ANXA1 (siANXA1) decreased the ANXA1 protein level by 59% for A375-MA2 and by 53% for SK-MEL-28, compared with the control siRNA (siCTRL, Supplementary Figure 1). Both cell lines transfected with siANXA1 presented reduced cell viability compared with cells transfected with siCTRL. This reduction started 48 hours after transfection for A375-MA2 and 72 hours after transfection for SK-MEL-28 (**Figure 2A** and **2E**). This decrease is linked to a decline in cell proliferation (**Figure 2B** and **2F**), with a significant reduction of PCNA in A375-MA2 (48 hours post-transfection) and an almost significant reduction in SK-MEL-28 (72 hours post-transfection, P=0.0559). To overcome this proliferation decrease following siANXA1 transfection, we performed a migration assay in a medium with limited serum (1%) for 24 hours. In siANXA1 conditions, we observed a significant reduction of migration after 16 hours in SK-MEL-28 only (**Figure 2C** and **2G**). Unlike siANXA1, the Ac2-26 peptide, which is widely used for its capacity to mimic the ANXA1 Nter domain, did not affect cell viability (Supplementary Figure 2). We therefore used complete medium for migration assays and extended the study time for A375-MA2 cells, which migrate more slowly than SK-MEL-28 cells. In these conditions, the peptide stimulated A375-MA2 migration only (**Figure 2D** and **2H**). Taken together, our findings indicate that manipulating cellular and external levels of ANXA1 can have contradictory effects on migration, depending on the melanoma cell line. However, regarding siRNA, ANXA1 has a booster effect on melanoma proliferation.

Stromal ANXA1 is involved in melanoma growth and metastatic capacity

To document the role of stromal ANXA1 in melanoma dissemination, we used B16Bl6 expressing a high level of ANXA1 (**Figure 3A**) grafted on C57Bl6/J WT and *Anxa1*-KO mice. As shown in **Figure 3B**, tumor apparition was delayed in the KO mice, with only 20% of tumors measurable using the caliper nine days after cell injection, compared with 80% in the WT mice. Tumor volumes were significantly reduced and growth was slower in the KO mice than in their WT counterparts (**Figure 3C** and **3E**). This is consistent with the tumor weight values at the time of sacrifice (**Figure 3D**). Next, we explored lung metastases in both types of mice. As shown in **Figure 3F** and **3G**, the KO mice were less likely to develop lung metastases and to a lesser extent than the WT mice. To further examine the involvement of stromal ANXA1 in dissemination, we injected B16Bl6 cells expressing the luciferase gene (B16Bl6-luc) intravenously into both types of mice. Although statistical significance was not reached, we observed a tendency towards lower relative radiance in the lungs of the mice without ANXA1 (**Figure 3H**). Altogether, these results indicate that ANXA1 from stromal cells is important for both melanoma development and dissemination *in vivo*.

Molecular mechanisms involved in melanoma growth and spreading related to ANXA1 stromal content

We first observed a decrease in the proliferation of KO mouse tumors, which displayed a slight but significant decrease of Ki67 positive nuclei compared with those of WT mice (**Figure 4A**). This could explain the smaller tumors in KO mice (**Figure 3C** and **3D**) and suggests that stromal ANXA1 might stimulate tumor prolifera-

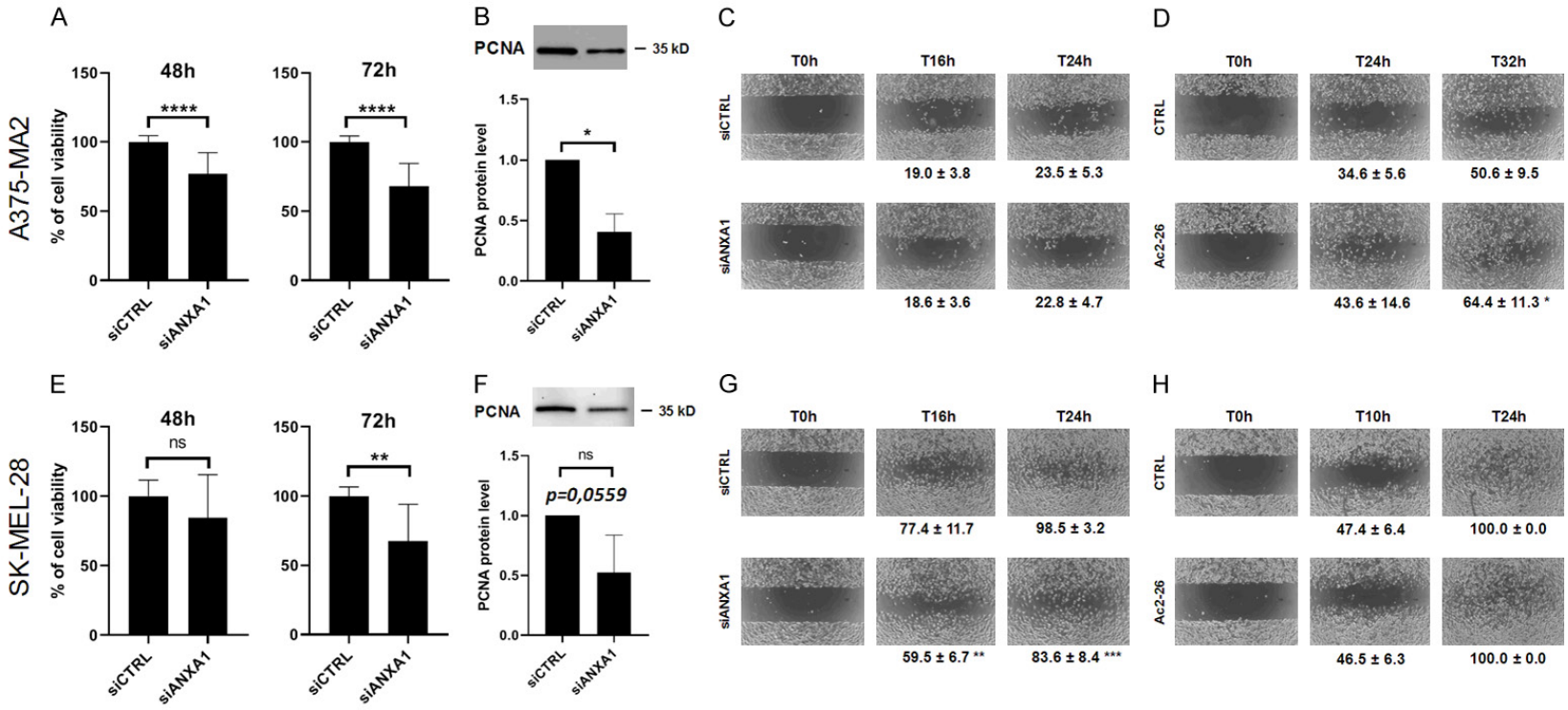

Figure 2. ANXA1 influences cell proliferation and migration. (A, E) Cytotoxicity analysis at 48 h and 72 h after cell transfection (siANXA1 or siCTRL). (B, F) PCNA level assessed using western blot to evaluate proliferation at 48 h (B) and 72 h (F) post-transfection. Total proteins were used as a loading control. (C, D, G, H) Migration abilities analysis of cells transfected with control or ANXA1 siRNA (C, G) or treated or not with Ac2-26 peptide (10 µM) (D, H). Percentage of wound closure ± standard deviation is indicated below the photos and were measured as described in methods sections. All experiments were repeated at least three times. Statistical significance was determined using Mann Whitney test (A, C-E, G, H) and one sample t-test (B, F) was realized with Ha: µ=1 as hypothetical, *P<0.05; **P<0.01; ***P<0.001; ****P<0.0001; ns, not significant.

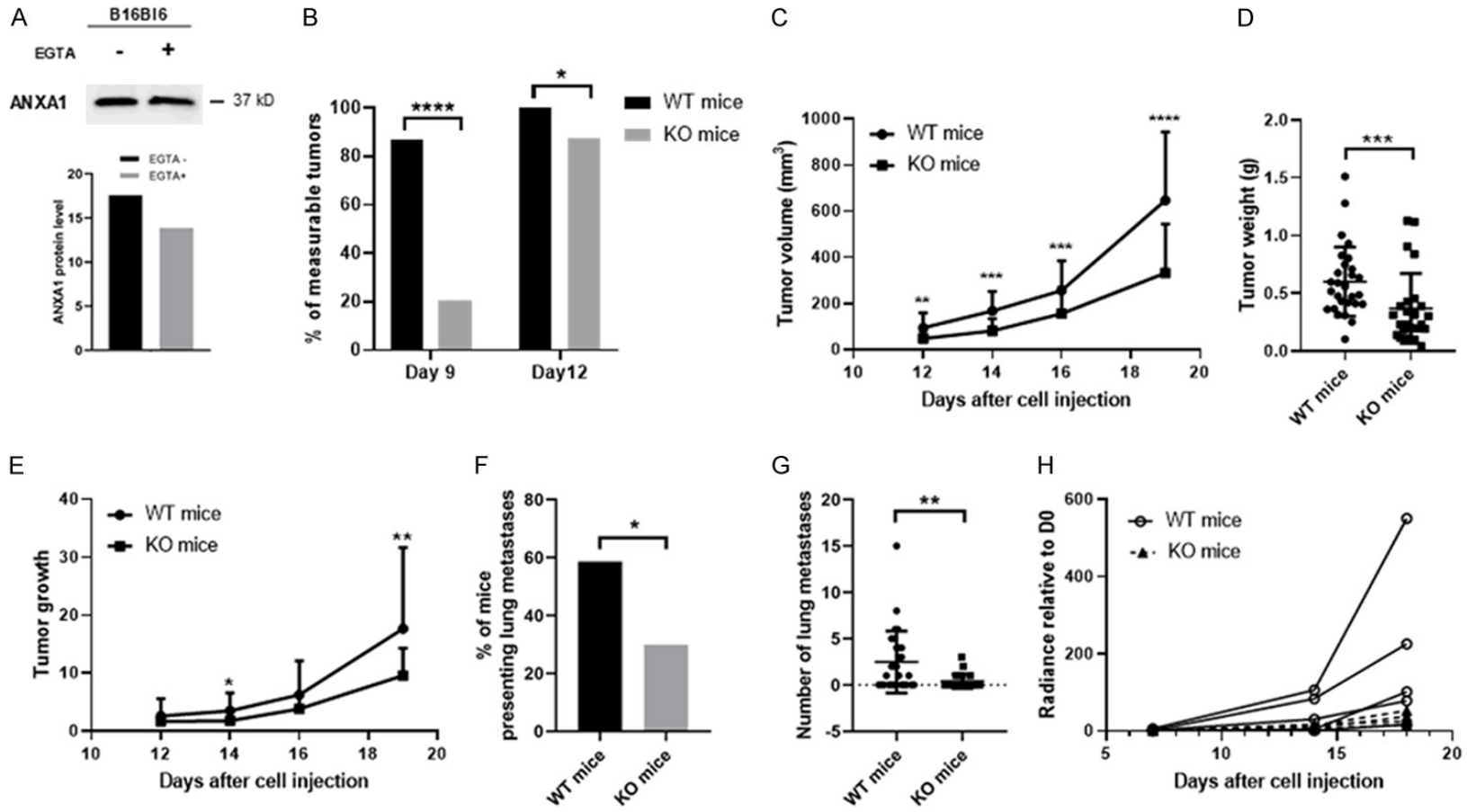

Figure 3. Stromal ANXA1 depletion limits melanoma tumor growth and metastasis. B16BI6 cells were injected subcutaneously in the flank of C57BI6/J WT or *Anxa1* KO mice. (A) Western blot analysis of ANXA1 level in B16BL6 cell line (B) The percentage of mice presenting a measurable tumor was determined for tumor establishment at day 9 and 12 after cell injection. (C) Evolution of tumor volume. Measurements were realized three times a week using a caliper as described in method section. (D) Tumor weight at day 19 post cell injection. (E) Evolution of tumor growth. (F) Percentage of mice presenting lung surfaces metastasis. (G) Number of lung metastasis. The data group two independent experiments, the first with 19 WT and 15 KO mice and the second with 10 WT and 10 KO mice. Statistical significance was determined using Chi-square (B, F) and Mann Whitney's test (C-E, G), *P<0.05; **P<0.01; ***P<0.001; ****P<0.0001. (H) B16BI6-luc cells were injected intravenously in the caudal vein of C57BI6 WT (n=5) or KO mice (n=4). Evolution of lung radiance relative to D0 which corresponds to cell injection was monitored weekly; each line corresponds to one mouse.

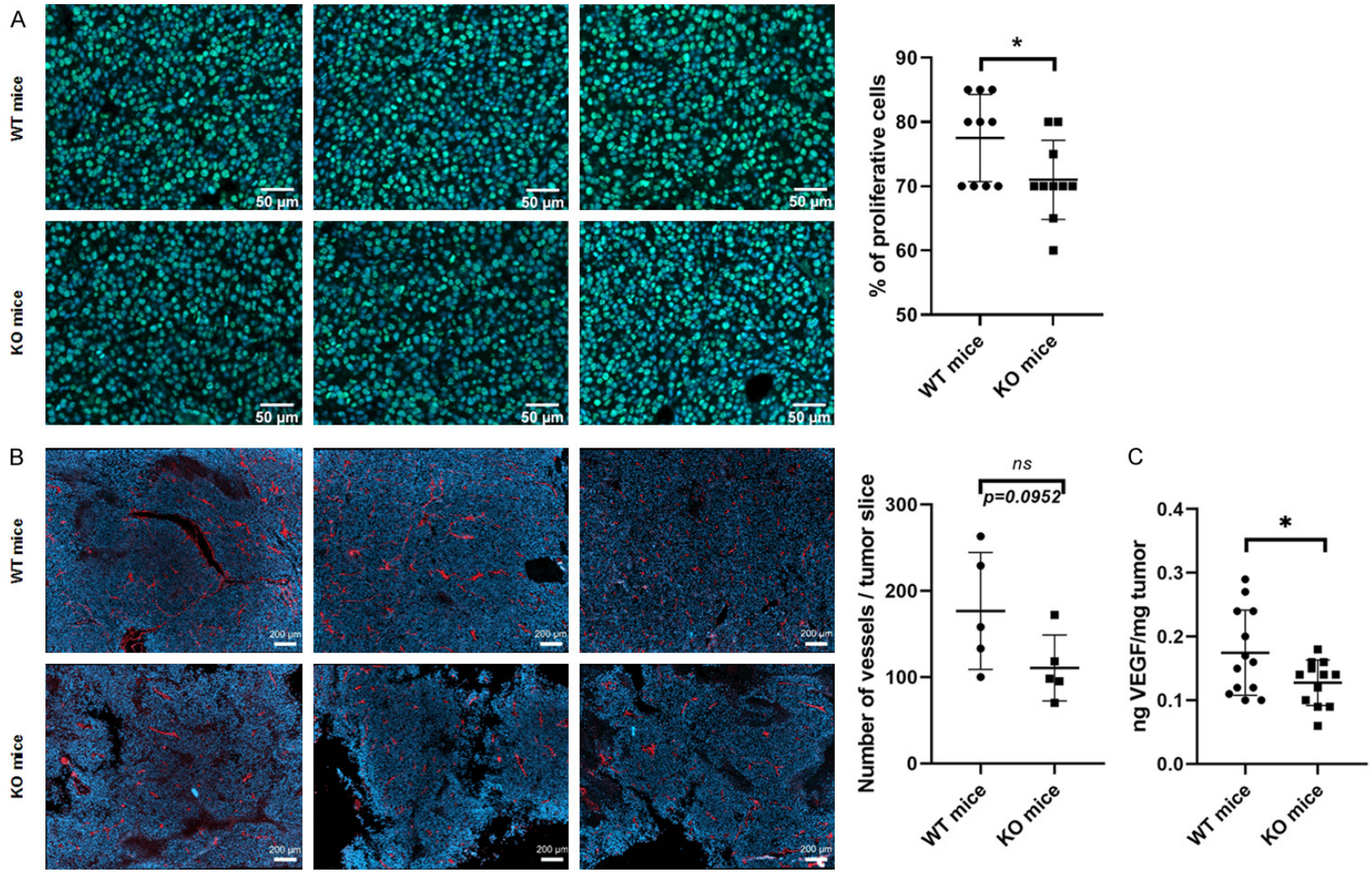

Figure 4. Stromal ANXA1 depletion reduces B16BI6 tumor proliferation and angiogenesis. (A) Immunofluorescence labelling was used to detect Ki-67 and assess tumor proliferation. Dot blot represents the percentage of nuclei labelled with Ki-67 and group two different experiments together, each with 5 tumors of WT and 5 of KO mice. (B) Immunofluorescence labelling was used to detect CD31 and assess tumor vessel density (WT n=5, KO n=5). Dot blot represents the number of vessels estimated from tumor slice. (A, B) Nuclei were labelled using Hoechst 33342 solution and merge images from three tumors are presented. Image represents a 4×4 mosaic realized at ×20 magnification, bars are equivalent to 50 µm (A, zoom) and 200 µm (B). (C) VEGF level in B16BI6 tumors of WT (n=13) and KO mice (n=12) was determined using ELISA assay. Dot blot represents mean ± standard deviation. Student's t-test with Welch's correction was realized to assess statistical significance, *P<0.05.

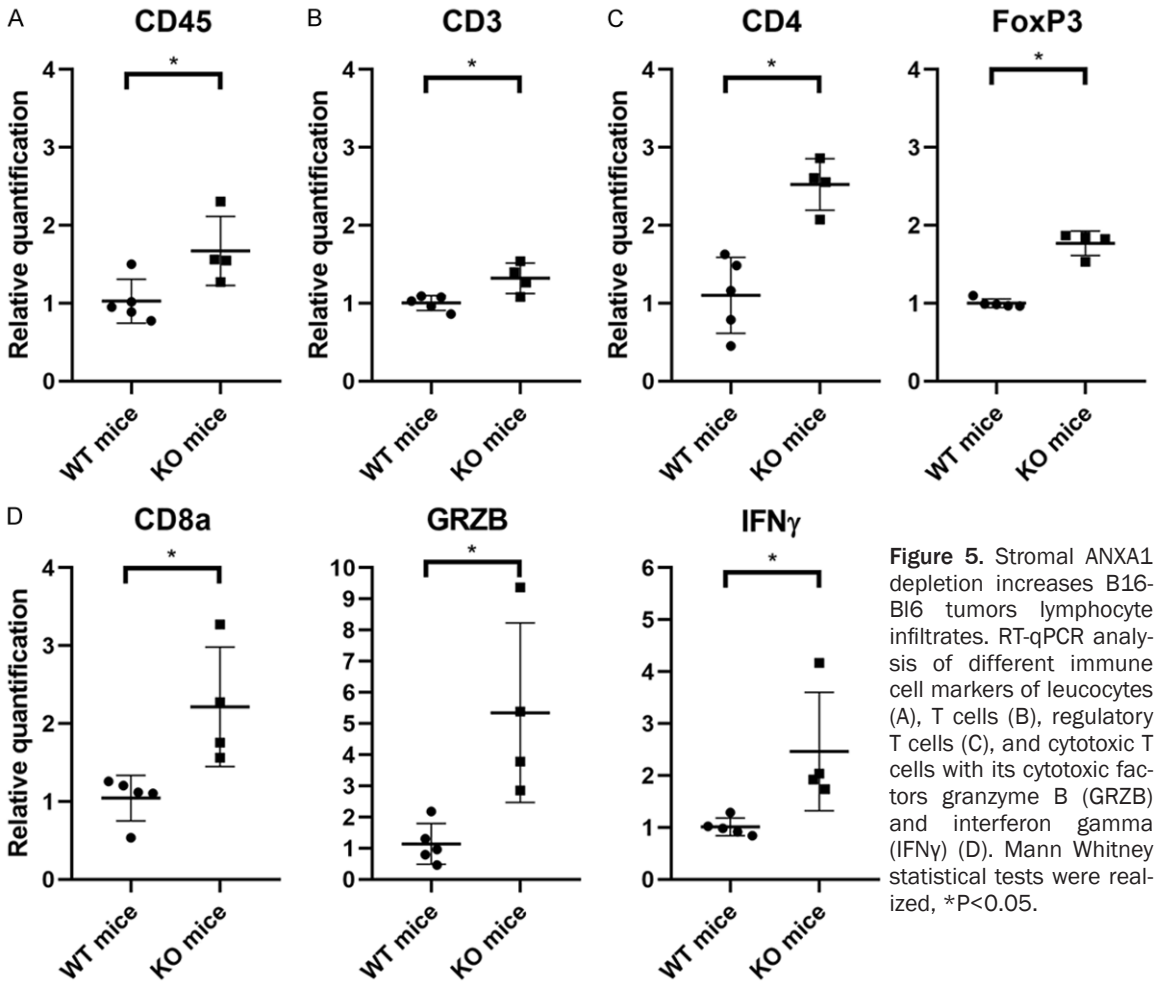

Figure 5. Stromal ANXA1 depletion increases B16-Bl6 tumors lymphocyte infiltrates. RT-qPCR analysis of different immune cell markers of leucocytes (A), T cells (B), regulatory T cells (C), and cytotoxic T cells with its cytotoxic factors granzyme B (GRZB) and interferon gamma (IFNγ) (D). Mann Whitney statistical tests were realized, *P<0.05.

tion. The differences in the development and formation of lung metastases between WT and KO mice could also be explained by altered angiogenesis. We analyzed the CD31 endothelial marker and VEGF dosage in the tumors (**Figure 4B** and **4C**). The tumors of KO mice had fewer vessels than WT mice tumors, as shown by CD31 labelling (**Figure 4B**). Moreover, VEGF was significantly increased in the tumors of WT mice (**Figure 4C**). These findings show that tumor angiogenesis was reduced in the mice lacking *Anxa1* expression. Hence, stromal ANXA1 seems to be a stimulating factor of tumor angiogenesis.

Absence of stromal ANXA1 associated with increased immune infiltrates

Several markers of immune cells were analyzed by RT-qPCR in the B16Bl6 tumors of WT and KO mice. As illustrated in **Figure 5A**, KO mouse tumors presented significantly more abundant leukocyte infiltrates compared with WT mice, as shown by overexpression of the CD45 marker. Although not significant, expression of the macrophage marker ADRE1, also called EMR1 or F4/80, was stronger in the KO mice, as was the expression of NKP46, indicating the presence of NK cells (data not shown, available upon request). However, the T lymphocyte marker CD3 was significantly more present in the melanoma tumors that developed in the KO mice than in those developed by the WT mice (**Figure 5B**). To develop this observation further, we examined the genes expressed by the cytotoxic and pro-tumoral lymphocytes. Both pro- and anti-tumor immune cells were significantly more present in the tumors of the KO mice. Regulatory T cell (Treg) markers (CD4 and FoxP3) were actually more abundant in the B16Bl6 tumors developed by the KO mice, as was the cytotoxic marker CD8a

(**Figure 5C** and **5D**). Furthermore, cytotoxic factors released by cytotoxic lymphocytes, granzyme B (GRZB) and interferon gamma (IFNγ) were also over-represented in the tumors of the KO mice compared with those of the WT mice (**Figure 5D**). Altogether, these results suggest that the absence of stromal ANXA1 generates a non-specific influx of immune cells, especially lymphocytes, in melanoma tumors.

Discussion

ANXA1 expression has generated significant interest as a biomarker in oncology. Despite numerous studies, its exact role in the mechanisms leading to tumor development and dissemination remains unclear and sometimes controversial [20]. We therefore focused our study on improving our understanding of the specific involvement of tumor and non-tumor ANXA1 in melanoma progression *in vitro* and *in vivo*. We had already showed that ANXA1 is overexpressed in melanoma cell lines compared with melanocytes [12, 21]. Here, we demonstrate the complexity of its role on two additional cell lines, SK-MEL-28 and A375-MA2, presenting high levels of ANXA1. While proliferation is affected by ANXA1 siRNA transfection in both cell lines, migration assays provide cell-dependent results. Indeed, siANXA1 only limited the migration of SK-MEL-28 and not that of A375-MA2, while the Ac2-26 peptide only enhanced the migration of A375-MA2. As SK-MEL-28 migrated more quickly than A375-MA2, it might be easier to observe a decline in cell migration in SK-MEL-28. The disparate results with the peptide could be due to the increased presence of secreted and cleaved forms of ANXA1 in SK-MEL-28 cells. The secreted bioactive peptide might actually compete with the exogenous peptide and limit its effects. However, in 2014, Belvedere and coworkers showed that the peptide is effective in stimulating migration of both types of cells regardless of ANXA1 secretion (MIA PaCa-2 and PANC-1 cells, respectively) [22]. FPR1 receptors were present in both cases. Our CMF analysis of FPR2 expression revealed that SK-MEL-28 and A375-MA2 cells expressed low basal levels of the receptor with around 15% (MFI=273) and 7.5% (MFI=149) of labelled cells, respectively (data not shown). Several studies of expression modulation and/or peptide mimicking stimulation performed on migration to date have shown the booster role of ANXA1 on this phenomenon in pancreatic [15, 22, 23], hepatic [24], nasopharyngeal [25], lung [26], gastric [27], esophageal [28] and breast cancers [29-31]. It therefore remains important to further improve our understanding of the involvement of ANXA1 in melanoma migration. As far as proliferation is concerned, heterogeneous results were obtained: for example, ANXA1 stimulated the proliferation of lung [26] and esophageal [28] cancer cells but showed anti-proliferative effects in pancreatic [15], stomach [32], breast cancers [33, 34] and oral squamous cell carcinoma [35]. In melanoma, our results suggest that ANXA1 stimulates proliferation. Further studies should be performed to pinpoint its role in cell viability.

The B16Bl6 graft on the *Anxa1* KO mice model allowed assessment of the role of the non-tumor domain of ANXA1 in tumor development and dissemination *in vivo*. For the first time, we demonstrated that stromal ANXA1 is important for both tumor growth and the formation of metastases in the B16Bl6 model. In fact, the absence of ANXA1 in the host generated a significant decrease in tumor proliferation and vascularization, associated with increased immune infiltrates. We hypothesize that the reduced tumor vascularization in the absence of stromal ANXA1 is responsible for limiting both tumor development and the formation of lung metastases. Indeed, tumor cells need oxygen and nutrients to grow and a dissemination path to reach secondary organs. In 2009, Yi and Schnitzer reported lower vessel density in B16 tumors (without ANXA1 expression) developed in *Anxa1* KO compared with WT mice, this being associated with decreased tumor volumes and increased necrosis [17]. We did also observe a decrease in vessel density in line with a reduction of the VEGF factor in the tumors developed by *Anxa1* KO mice. There is no clear relationship concerning the effect of ANXA1 on VEGF expression, although VEGF can modulate ANXA1 expression. For instance, in endothelial cells, VEGF expression decreases miRNA-196a, which destabilizes 3'UTR ANXA1 mRNA, showing a positive correlation between VEGF and ANXA1 [36]. Hypoxia can also increase ANXA1 expression and its external location suggests a close link between angiogenesis and ANXA1 [37]. Our RT-qPCR analyses (not shown), as well as previously published results

[17], show that VEGF expression is similar in tumors developed in WT and *Anxa1* KO mice in melanoma models, suggesting regulation of protein levels. Therefore, we hypothesize that stromal ANXA1 could modulate the production and/or secretion of VEGF by the cells of the tumor's microenvironment. A recent publication not related to cancer describes the action of ANXA1 on VEGF production via binding to FPR2, and subsequent ERK activation in uterine epithelial cells [38]. Furthermore, another study shows that cardiac macrophages from *Anxa1* KO mice exhibit a reduced ability to release VEGF [39].

Another parameter that can impact angiogenesis in the KO mice is the characteristic presence of ANXA1 in tumor endothelial cells, reported by several studies including the pioneering publication by Oh et al [18] and Allen et al's more recent contribution [40]. Although the precise role of ANXA1 in endothelial cells is not fully understood, Cristante and colleagues highlighted the importance of ANXA1 in the paracellular permeability of brain endothelial cells [41]. The human brain endothelial cells that did not express ANXA1 had a higher paracellular permeability than those that did express the protein. This increased permeability is associated with the decreased expression of junction proteins, such as occludin and VE-Cadherin [41]. A future study comparing endothelial junction protein patterns in the tumors of WT and KO mice would be pertinent.

It might then be possible to propose that the increased tumor immune infiltrates in KO mice could be a consequence of leaky vasculature rather than direct action on immune cells due to the lack of stromal ANXA1. Indeed, both anti- and pro-tumoral immune cells are upregulated in the tumors of KO mice. It is well known that tumor vessels present more leaks than normal vessels [42]. Given the tumor reduction and the limited formation of metastases, we suppose that anti-tumor immune cells are abundant enough to contain tumor proliferation and dissemination. We can also note that there is no direct, clear association between tumor volume and aggressiveness for human melanomas, which confirms our previous results. We have ruled out apoptosis and immunogenic cell deaths which can be immune stimulators (data not shown). A non-exclusive possibility remains with increased inflammation indicated by increased TNF alpha and Il12 in the tumors developed by Anxa1 KO mice (data not shown). Further experiments are needed to highlight this original observation. The involvement of stromal ANXA1 in tumor dissemination has also been reported in other types of cancer with *Anxa1* KO animal models, such as lung [17] and breast cancers [16, 43]. In these models, the absence of ANXA1 in the host limited the development of metastases, as shown in our melanoma model. However, the results concerning tumor volumes are more heterogeneous. In syngeneic models of melanoma [17], lung [17] and breast cancers [16], the absence of stromal ANXA1 decreased tumor volumes. However, in chemically-induced [44] or in spontaneous model [43] breast cancers, the absence of stromal ANXA1 increased tumor volumes. Taken together, these results confirm that ANXA1 from non-tumor cells is important for both tumor development and metastases in syngenic models. On the other hand, studies with WT mice grafted with *Anxa1* KO tumor cells or depleted for ANXA1 show that tumor ANXA1 only affected the metastases, stimulating their formation. This has been shown in pancreas [15], stomach [27], breast [14] and nasopharyngeal cancers [25]. Our team has already demonstrated, via intra-tumoral injection of siANXA1 in B16Bl6 tumors, that ANXA1 from tumor cells stimulates the formation of lung metastases [12]. The main issue concerning the role of ANXA1 in tumors, and specifically in melanomas, remains the clarification of the role of this anti-inflammatory protein in tumor progression according to its tumor or non-tumor location. The generation of specific and stable ANXA1 KO cells using CRISPR-Cas9 technology may help to confirm the involvement of tumoral ANXA1 in the formation of metastases.

To sum up, our study reports new insight into tumor and non-tumor ANXA1 in melanoma progression. While the role of tumor ANXA1 requires further analysis, stromal ANXA1 is clearly involved in both melanoma development and metastases *in vivo*, possibly through angiogenesis modulation. These findings sustain the interest in studying the role of ANXA1 and potential targeting in melanoma.

Acknowledgements

We would like to express our gratitude to Ms. Christelle Blavignac from the Cell Imaging

Center of Clermont Auvergne University and Ms. Christelle Damon-Soubeyrand from the histopathology platform (Anipath, GReD), for their assistance with the flow-cytometry and immunofluorescence assays, respectively.

Disclosure of conflict of interest

None.

Address correspondence to: Dr. Françoise Degoul, Université Clermont Auvergne, INSERM, Imagerie Moléculaire et Stratégies Théranostiques, UMR-1240, 58 Rue Montalembert, Clermont-Ferrand Cedex 63005, France. Tel: +33 (0)4 73 15 08 14; E-mail: francoise.degoul@inserm.fr

References

[1] Perretti M and D'Acquisto F. Annexin A1 and glucocorticoids as effectors of the resolution of inflammation. Nat Rev Immunol 2009; 9: 62-70.

[2] McArthur S, Juban G, Gobbetti T, Desgeorges T, Theret M, Gondin J, Toller-Kawahisa JE, Reutelingsperger CP, Chazaud B, Perretti M and Mounier R. Annexin A1 drives macrophage skewing to accelerate muscle regeneration through AMPK activation. J Clin Invest 2020; 130: 1156-1167.

[3] D'Acquisto F. On the adaptive nature of annexin-A1. Curr Opin Pharmacol 2009; 9: 521-528.

[4] Tzelepis F, Verway M, Daoud J, Gillard J, Hassani-Ardakani K, Dunn J, Downey J, Gentile ME, Jaworska J, Sanchez AM, Nedelec Y, Vali H, Tabrizian M, Kristof AS, King IL, Barreiro LB and Divangahi M. Annexin1 regulates DC efferocytosis and cross-presentation during Mycobacterium tuberculosis infection. J Clin Invest 2015; 125: 752-768.

[5] Baracco EE, Stoll G, Van Endert P, Zitvogel L, Vacchelli E and Kroemer G. Contribution of annexin A1 to anticancer immunosurveillance. Oncoimmunology 2019; 8: e1647760.

[6] Baracco EE, Petrazzuolo A and Kroemer G. Assessment of annexin A1 release during immunogenic cell death. Methods Enzymol 2019; 629: 71-79.

[7] Rouanet J, Benboubker V, Akil H, Hennino A, Auzeloux P, Besse S, Pereira B, Delorme S, Mansard S, D'Incan M, Degoul F and Rouzaire PO. Immune checkpoint inhibitors reverse tolerogenic mechanisms induced by melanoma targeted radionuclide therapy. Cancer Immunol Immunother 2020; 69: 2075-2088.

[8] Galluzzi L, Buque A, Kepp O, Zitvogel L and Kroemer G. Immunogenic cell death in cancer and infectious disease. Nat Rev Immunol 2017; 17: 97-111.

[9] Foo SL, Yap G, Cui J and Lim LHK. Annexin-A1-a blessing or a curse in cancer? Trends Mol Med 2019; 25: 315-327.

[10] Tu Y, Johnstone CN and Stewart AG. Annexin A1 influences in breast cancer: controversies on contributions to tumour, host and immunoediting processes. Pharmacol Res 2017; 119: 278-288.

[11] Rondepierre F, Bouchon B, Papon J, Bonnet-Duquennoy M, Kintossou R, Moins N, Maublant J, Madelmont JC, D'Incan M and Degoul F. Proteomic studies of B16 lines: involvement of annexin A1 in melanoma dissemination. Biochim Biophys Acta 2009; 1794: 61-69.

[12] Boudhraa Z, Rondepierre F, Ouchchane L, Kintossou R, Trzeciakiewicz A, Franck F, Kanitakis J, Labeille B, Joubert-Zakeyh J, Bouchon B, Perrot JL, Mansard S, Papon J, Dechelotte P, Chezal JM, Miot-Noirault E, Bonnet M, D'Incan M and Degoul F. Annexin A1 in primary tumors promotes melanoma dissemination. Clin Exp Metastasis 2014; 31: 749-760.

[13] Boudhraa Z, Bouchon B, Viallard C, D'Incan M and Degoul F. Annexin A1 localization and its relevance to cancer. Clin Sci (Lond) 2016; 130: 205-220.

[14] de Graauw M, van Miltenburg MH, Schmidt MK, Pont C, Lalai R, Kartopawiro J, Pardali E, Le Dévédec SE, Smit VT, van der Wal A, Van't Veer LJ, Cleton-Jansen AM, ten Dijke P and van de Water B. Annexin A1 regulates TGF-beta signaling and promotes metastasis formation of basal-like breast cancer cells. Proc Natl Acad Sci U S A 2010; 107: 6340-6345.

[15] Belvedere R, Bizzarro V, Forte G, Dal Piaz F, Parente L and Petrella A. Annexin A1 contributes to pancreatic cancer cell phenotype, behaviour and metastatic potential independently of formyl peptide receptor pathway. Sci Rep 2016; 6: 29660.

[16] Moraes LA, Kar S, Foo SL, Gu T, Toh YQ, Ampomah PB, Sachaphibulkij K, Yap G, Zharkova O, Lukman HM, Fairhurst AM, Kumar AP and Lim LHK. Annexin-A1 enhances breast cancer growth and migration by promoting alternative macrophage polarization in the tumour microenvironment. Sci Rep 2017; 7: 17925.

[17] Yi M and Schnitzer JE. Impaired tumor growth, metastasis, angiogenesis and wound healing in annexin A1-null mice. Proc Natl Acad Sci U S A 2009; 106: 17886-17891.

[18] Oh P, Li Y, Yu J, Durr E, Krasinska KM, Carver LA, Testa JE and Schnitzer JE. Subtractive proteomic mapping of the endothelial surface in lung and solid tumours for tissue-specific therapy. Nature 2004; 429: 629-635.

[19] Hannon R, Croxtall JD, Getting SJ, Roviezzo F, Yona S, Paul-Clark MJ, Gavins FN, Perretti M, Morris JF, Buckingham JC and Flower RJ. Aberrant inflammation and resistance to glucocorticoids in annexin 1-/- mouse. FASEB J 2003; 17: 253-255.

[20] Fu Z, Zhang S, Wang B, Huang W, Zheng L and Cheng A. Annexin A1: a double-edged sword as novel cancer biomarker. Clin Chim Acta 2020; 504: 36-42.

[21] Caputo E, Maiorana L, Vasta V, Pezzino FM, Sunkara S, Wynne K, Elia G, Marincola FM, McCubrey JA, Libra M, Travali S and Kane M. Characterization of human melanoma cell lines and melanocytes by proteome analysis. Cell Cycle 2011; 10: 2924-2936.

[22] Belvedere R, Bizzarro V, Popolo A, Dal Piaz F, Vasaturo M, Picardi P, Parente L and Petrella A. Role of intracellular and extracellular annexin A1 in migration and invasion of human pancreatic carcinoma cells. BMC Cancer 2014; 14: 961.

[23] Pessolano E, Belvedere R, Bizzarro V, Franco P, Marco I, Petrella F, Porta A, Tosco A, Parente L, Perretti M and Petrella A. Annexin A1 contained in extracellular vesicles promotes the activation of keratinocytes by mesoglycan effects: an autocrine loop through FPRs. Cells 2019; 8: 753.

[24] Lin Y, Lin G, Fang W, Zhu H and Chu K. Increased expression of annexin A1 predicts poor prognosis in human hepatocellular carcinoma and enhances cell malignant phenotype. Med Oncol 2014; 31: 327.

[25] Zhu JF, Huang W, Yi HM, Xiao T, Li JY, Feng J, Yi H, Lu SS, Li XH, Lu RH, He QY and Xiao ZQ. Annexin A1-suppressed autophagy promotes nasopharyngeal carcinoma cell invasion and metastasis by PI3K/AKT signaling activation. Cell Death Dis 2018; 9: 1154.

[26] Guan X, Fang Y, Long J and Zhang Y. Annexin 1-nuclear factor-kappaB-microRNA-26a regulatory pathway in the metastasis of non-small cell lung cancer. Thorac Cancer 2019; 10: 665-675.

[27] Cheng TY, Wu MS, Lin JT, Lin MT, Shun CT, Huang HY, Hua KT and Kuo ML. Annexin A1 is associated with gastric cancer survival and promotes gastric cancer cell invasiveness through the formyl peptide receptor/extracellular signal-regulated kinase/integrin beta-1-binding protein 1 pathway. Cancer 2012; 118: 5757-5767.

[28] Han G, Lu K, Huang J, Ye J, Dai S, Ye Y and Zhang L. Effect of Annexin A1 gene on the proliferation and invasion of esophageal squamous cell carcinoma cells and its regulatory mechanisms. Int J Mol Med 2017; 39: 357-363.

[29] Vecchi L, Alves Pereira Zóia M, Goss Santos T, de Oliveira Beserra A, Colaço Ramos CM, França Matias Colombo B, Paiva Maia YC, Piana de Andrade V, Teixeira Soares Mota S, Gonçalves de Araújo T, Van Petten de Vasconcelos Azevedo F, Soares FA, Oliani SM and Goulart LR. Inhibition of the AnxA1/FPR1 autocrine axis reduces MDA-MB-231 breast cancer cell growth and aggressiveness in vitro and in vivo. Biochim Biophys Acta Mol Cell Res 2018; 1865: 1368-1382.

[30] Bhardwaj A, Ganesan N, Tachibana K, Rajapakshe K, Albarracin CT, Gunaratne PH, Coarfa C and Bedrosian I. Annexin A1 preferentially predicts poor prognosis of basal-like breast cancer patients by activating mTOR-S6 signaling. PLoS One 2015; 10: e0127678.

[31] Kang H, Ko J and Jang SW. The role of annexin A1 in expression of matrix metalloproteinase-9 and invasion of breast cancer cells. Biochem Biophys Res Commun 2012; 423: 188-194.

[32] Gao Y, Chen Y, Xu D, Wang J and Yu G. Differential expression of ANXA1 in benign human gastrointestinal tissues and cancers. BMC Cancer 2014; 14: 520.

[33] Yuan Y, Anbalagan D, Lee LH, Samy RP, Shanmugam MK, Kumar AP, Sethi G, Lobie PE and Lim LH. ANXA1 inhibits miRNA-196a in a negative feedback loop through NF-kB and c-Myc to reduce breast cancer proliferation. Oncotarget 2016; 7: 27007-27020.

[34] Bist P, Phua QH, Shu S, Yi Y, Anbalagan D, Lee LH, Sethi G, Low BC and Lim LH. Annexin-A1 controls an ERK-RhoA-NFkappaB activation loop in breast cancer cells. Biochem Biophys Res Commun 2015; 461: 47-53.

[35] Wan YM, Tian J, Qi L, Liu LM and Xu N. ANXA1 affects cell proliferation, invasion and epithelial-mesenchymal transition of oral squamous cell carcinoma. Exp Ther Med 2017; 14: 5214-5218.

[36] Pin AL, Houle F, Fournier P, Guillonneau M, Paquet ER, Simard MJ, Royal I and Huot J. Annexin-1-mediated endothelial cell migration and angiogenesis are regulated by vascular endothelial growth factor (VEGF)-induced inhibition of miR-196a expression. J Biol Chem 2012; 287: 30541-30551.

[37] Bizzarro V, Belvedere R, Migliaro V, Romano E, Parente L and Petrella A. Hypoxia regulates ANXA1 expression to support prostate cancer cell invasion and aggressiveness. Cell Adh Migr 2017; 11: 247-260.

[38] Hebeda CB, Sandri S, Benis CM, Paula-Silva M, Loiola RA, Reutelingsperger C, Perretti M and Farsky SHP. Annexin A1/formyl peptide receptor pathway controls uterine receptivity to the blastocyst. Cells 2020; 9: 1188.

[39] Ferraro B, Leoni G, Hinkel R, Ormanns S, Paulin N, Ortega-Gomez A, Viola JR, de Jong R, Bongiovanni D, Bozoglu T, Maas SL, D'Amico M, Kessler T, Zeller T, Hristov M, Reutelingsperger C, Sager HB, Doring Y, Nahrendorf M, Kupatt C and Soehnlein O. Pro-angiogenic macrophage phenotype to promote myocardial repair. J Am Coll Cardiol 2019; 73: 2990-3002.

[40] Allen KL, Cann J, Zhao W, Peterson N, Lazzaro M, Zhong H, Wu H, Dall'Acqua WF, Borrok MJ, Damschroder MM, Tsui P and Li Q. Upregulation of annexin A1 protein expression in the intratumoral vasculature of human non-small-cell lung carcinoma and rodent tumor models. PLoS One 2020; 15: e0234268.

[41] Cristante E, McArthur S, Mauro C, Maggioli E, Romero IA, Wylezinska-Arridge M, Couraud PO, Lopez-Tremoleda J, Christian HC, Weksler BB, Malaspina A and Solito E. Identification of an essential endogenous regulator of blood-brain barrier integrity, and its pathological and therapeutic implications. Proc Natl Acad Sci U S A 2013; 110: 832-841.

[42] Lugano R, Ramachandran M and Dimberg A. Tumor angiogenesis: causes, consequences, challenges and opportunities. Cell Mol Life Sci 2020; 77: 1745-1770.

[43] Bist P, Leow SC, Phua QH, Shu S, Zhuang Q, Loh WT, Nguyen TH, Zhou JB, Hooi SC and Lim LH. Annexin-1 interacts with NEMO and RIP1 to constitutively activate IKK complex and NF-kappaB: implication in breast cancer metastasis. Oncogene 2011; 30: 3174-3185.

[44] Ang EZ, Nguyen HT, Sim HL, Putti TC and Lim LH. Annexin-1 regulates growth arrest induced by high levels of estrogen in MCF-7 breast cancer cells. Mol Cancer Res 2009; 7: 266-274.

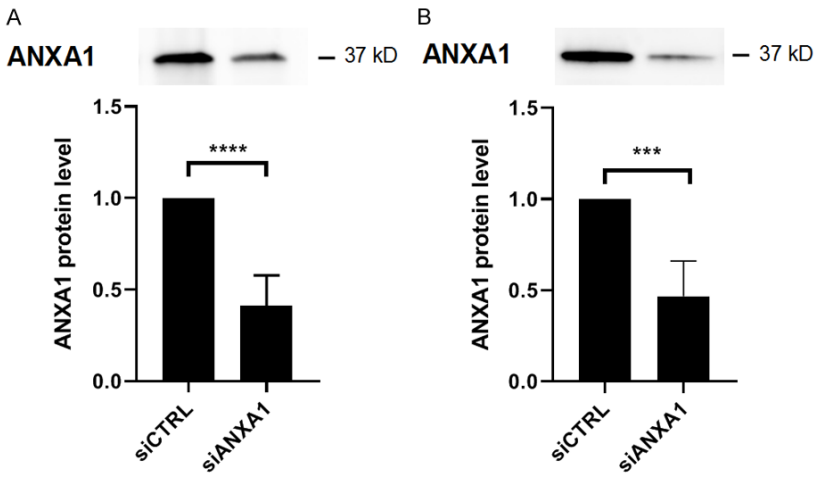

Supplementary Figure 1. Depletion of ANXA1 after cell transfection with siRNA. A375-MA2 (A) and SK-MEL-28 (B) cells were transfected with control or ANXA1 siRNA and 48 h later cell lysates were analyzed for ANXA1 protein level using western blot. Total proteins were used as a loading control and the ratio of ANXA1 level in siANXA1/siCTRL cells was done to estimate protein reduction. One sample t-test was realized with 1 as hypothetical value to assess significance, ***p<0.001, ****p<0.0001.

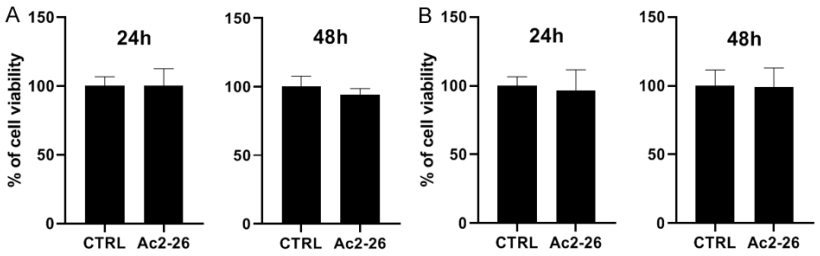

Supplementary Figure 2. Ac2-26 peptide has no effect on melanoma cells viability. A375-MA2 (A) and SK-MEL-28 (B) cells were treated with 10 μM of Ac2-26 peptide and then subjected to resazurin reduction to assess cytotoxicity 24 h and 48 h after treatment.